Accurate Small-Signal Model for an Automotive Bidirectional Dual Active Bridge Converter

F. Krismer, J. W. Kolar
Power Electronic Systems Laboratory, ETH Zurich, Switzerland
Email: krismer@lem.ee.ethz.ch

***Abstract*—The derivation of an accurate small-signal model for a galvanically isolated, bidirectional DC-DC converter and the implementation of a corresponding controller on a digital signal processor (DSP) as well as key methods and functions required for the digital implementation are detailed in this paper. The investigated DC-DC converter, an automotive Dual Active Bridge (DAB) system enables power transfer between a low voltage port (ranging from 11 V to 16 V) and a high voltage port (240 V to 450 V). The nominal power rating is 2 kW. The developed small-signal model yields highly accurate results for the DAB system, but the proposed modelling procedure could also be applied to arbitrary resonant power converters with unidirectional or bidirectional power transfer.**

I. Introduction

Accurate dynamic models for power converters are of great importance during the compensator design process in order to achieve a stable converter operation and a high control performance. Unfortunately, nonlinear components – such as switches and diodes – are inherent to switching power converters and thus the effort to derive system transfer functions is considerably higher than the work required for the analysis of linear systems.

For a power converter system with defined input and output control variables, the dynamic system behaviour typically depends on the operating point, which determines the steady state values of the characteristic system variables (e.g. inductor currents, capacitor voltages). A disturbance applied to any control input may deflect the characteristic system variables from their steady state values, which in turn causes the output variables to change. This change is typically linearized at the operating point in order to determine the small-signal transfer function. In the literature, a large number of different methods on how to obtain a small-signal converter model, is described. Well known methods are circuit averaging or state space averaging [1]. However, these two methods assume negligible current and voltage changes during the switching period T_S and can not be used for the investigated Dual Active Bridge (DAB) converter (**Figure 1**), since the currents in the required high frequency transformer change significantly during T_S. Thus, a method developed for resonant power converters [2] is employed for the DAB. With [2], a precise discrete time model results, which is perfectly suited for digital control.

The presented work discusses the derivation of a discrete time, small-signal model for a 2 kW bidirectional DAB converter with a low voltage (LV) port (V_1 ranging from 11 V to 16 V, nominal voltage: $V_1 = 12$ V) and a high voltage (HV) port (V_2 between 240 V and 450 V, nominal voltage: $V_2 = 340$ V) including EMI filters. It has been designed for a hybrid electric vehicle application in order to enable bidirectional energy transfer between the conventional 14-V power distribution system and the high voltage DC bus (e.g. in a power system architecture according to Fig. 2 in [3]). The DAB mode of operation is briefly described in **Section II**, the small-signal model is derived in **Section III**, and the employed control loop is discussed in **Section IV**.

Circuit Component	Value
C_{DC1}	20000 µF
R_{f1}	7 mΩ
L_{f1}	100 nH
C_{f1}	1000 µF
n	24
L	31 µH (phase shift modulation) or 20.6 µH (alternative modulation)
R	1.0 Ω
C_{f2}	3.3 µF
L_{f2a}	20 µH
R_{f2a}	10 mΩ
L_{f2b}	10 µH
R_{f2b}	3.1 Ω
C_{DC2}	100 µF

Table I: Values of the filter components in Fig. 1 for phase shift modulation and alternative modulation. Resistor R considers the DAB conduction losses and is connected in series to L [4]; resistor R_{f2a} is connected in series to L_{f2a} and models its copper losses.

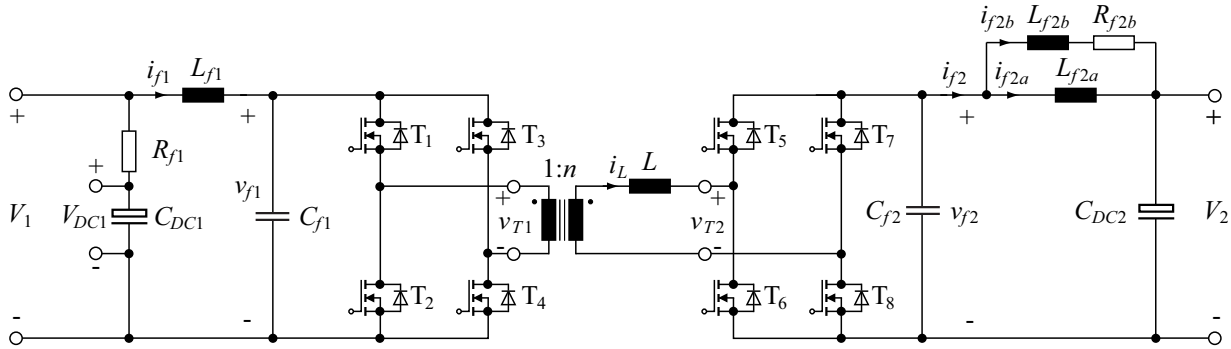

Figure 1: Dual active bridge (DAB) converter with low voltage (LV) and high voltage (HV) side EMI filters.

978-1-4244-2551-8/08/$20.00 ©2008 IEEE

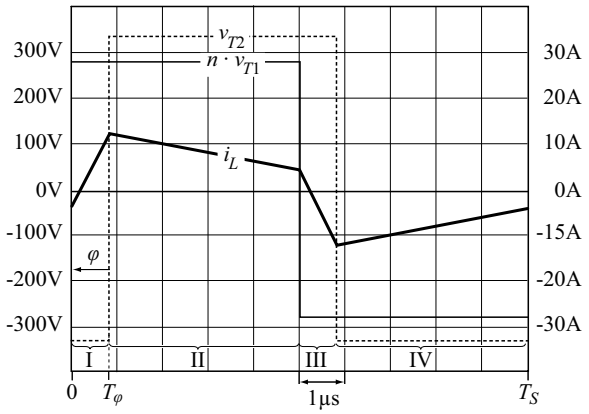

Figure 2: Transformer voltage and current waveforms for phase shift modulation and nominal operation ($V_1 = 12\,\mathrm{V}$, $V_2 = 340\,\mathrm{V}$, $P_2 = 2\,\mathrm{kW}$), $n = 24$, and power transfer from the LV to the HV port.

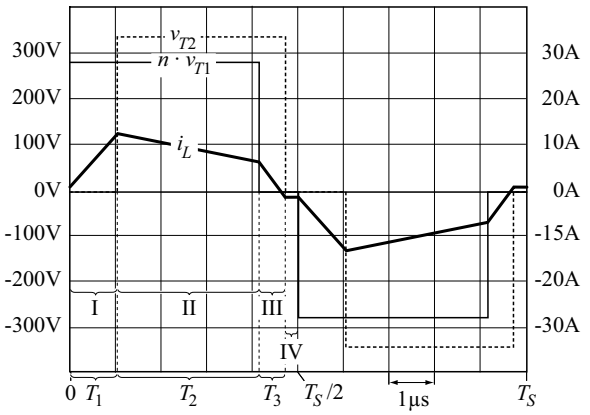

Figure 3: Transformer voltage and current waveforms for the alternative modulation and nominal operation with power transfer from the LV to the HV port. The inductor current i_L is slightly negative during time interval IV in order to enable HV side soft switching.

II. Converter

The investigated DAB converter in Figure 1 consists of two full bridge circuits, which are connected to a high frequency transformer and a converter inductor L. EMI filters are included on the low voltage side as well as on the high voltage side in order to meet the specified EMI requirements; the component values are listed in **Table I**, the employed switching frequency is $f_S = 100\,\mathrm{kHz}$.

In order for the DAB to transfer power, time varying voltages $v_{T1}(t)$ and $v_{T2}(t)$ must be provided from the full bridge circuits to the high frequency transformer and the converter inductor L. Possible values for $v_{T1}(t)$ are

$$v_{T1}(t) = \begin{cases} +v_{f1}(t) & \text{for } (\mathrm{T}_1, \mathrm{T}_4 \text{ on}, \mathrm{T}_2, \mathrm{T}_3 \text{ off}) \\ 0 & \text{for } (\mathrm{T}_1, \mathrm{T}_3 \text{ on}, \mathrm{T}_2, \mathrm{T}_4 \text{ off}) \text{ or } (\mathrm{T}_2, \mathrm{T}_4 \text{ on}, \mathrm{T}_1, \mathrm{T}_3 \text{ off}) \\ -v_{f1}(t) & \text{for } (\mathrm{T}_2, \mathrm{T}_3 \text{ on}, \mathrm{T}_1, \mathrm{T}_4 \text{ off}) \end{cases} \quad (1)$$

(provided that the full bridges are ideal; failure modes – e.g. bridge leg short circuits – are not considered). Similarly, $v_{T2}(t)$ is equal to one of $+v_{f2}(t)$, 0, and $-v_{f2}(t)$ depending on the switching states of T_5, T_6, T_7, and T_8. According to Figure 1, the voltage difference between $n \cdot v_{T1}(t)$ and $v_{T2}(t)$ appears across L which generates the current

$$i_L(t_1) = i_L(t_0) + \frac{1}{L}\int_{t_0}^{t_1} (n \cdot v_{T1}(t) - v_{T2}(t))\,\mathrm{d}t, \quad t_0 < t_1 \quad (2)$$

at the time t_1, starting with an initial current $i_L(t_0)$ at time t_0. The expressions for the instantaneous power on LV and HV side are

$$p_1(t) = n \cdot v_{T1}(t) \cdot i_L(t) \quad \text{and} \quad p_2(t) = v_{T2}(t) \cdot i_L(t)\,, \quad (3)$$

for the DAB without EMI filters and when transformer magnetization current and DAB converter losses are neglected. The average power values over one switching cycle $T_S = 1/f_S$ are finally calculated with

$$P_1 = \frac{1}{T_S}\int_{t_0}^{t_0+T_S} p_1(t)\mathrm{d}t \quad \text{and} \quad P_2 = \frac{1}{T_S}\int_{t_0}^{t_0+T_S} p_2(t)\mathrm{d}t\,. \quad (4)$$

Most often, one or more out of three main possibilities are employed to adjust the power level of the DAB converter:

- adjustment of the phase shift φ between $v_{T1}(t)$ and $v_{T2}(t)$,
- duty cycle modulation of $v_{T1}(t)$ and $v_{T2}(t)$,
- switching frequency variation.

The most common modulation principle, the so called "phase shift modulation" operates the DAB at constant switching frequency and only varies the phase shift φ in order to achieve the required power transfer. For phase shift modulation, maximum duty cycles are selected for $v_{T1}(t)$ and $v_{T2}(t)$, hence $v_{T1}(t)$ is either $-v_{f1}(t)$ or $v_{f1}(t)$ and $v_{T2}(t)$ is either $-v_{f2}(t)$ or $v_{f2}(t)$. Typical waveforms for the inductor current and the transformer voltages during one switching period are depicted in **Figure 2** when the DAB transfers power from the LV port to the HV port at the nominal operating point ($V_1 = 12\,\mathrm{V}$, $V_2 = 340\,\mathrm{V}$, $P_2 = 2\,\mathrm{kW}$). Obviously, the DC component of the inductor current vanishes over one switching cycle T_S, which is required in order to avoid saturation of the high frequency transformer. The inductor current repeats every half cycle with reversed sign, $i_L(t + T_S/2) = -i_L(t)$, since the phase shift time T_φ and the DC supply voltages V_1 and V_2 remain the same during the first and the second half cycle (time intervals I, II and III, IV in Figure 2, respectively). Therefore, only the first half cycle (intervals I and II for phase shift modulation) needs to be considered.

The great advantage of the phase shift modulation is its simplicity: only a single control variable, the phase shift angle φ, is required to arbitrarily transfer power according to

$$P_1 = P_2 = \frac{n \cdot V_1 \cdot V_2 \cdot \varphi \cdot (\pi - |\varphi|)}{2\pi^2 f_S L}, \; -\frac{\pi}{2} < \varphi < \frac{\pi}{2}. \quad (5)$$

Disadvantages of this modulation are the limited operating range where low switching losses occur (soft switching range, see [5]) and a large amount of reactive power in the high frequency transformer which may occur for certain working points when the DAB is operated within wide voltage ranges [6].

In order to increase the converter efficiency, an alternative modulation method has been investigated in [7] and [6], which not only adjusts the phase shift between $v_{T1}(t)$ and $v_{T2}(t)$ but as well changes the duty cycles. The resulting inductor current and the transformer voltages are depicted in **Figure 3** for the nominal operating point. This alternative modulation scheme enables significantly higher converter efficiency compared to phase shift modulation for most operating points within the given voltage ranges. The cost for better converter utilization is mainly the higher complexity: now a single half cycle consists of four different time intervals (compared to two different time intervals for phase shift modulation) which are simultaneously adjusted with three timing parameters T_1, T_2, and T_3.

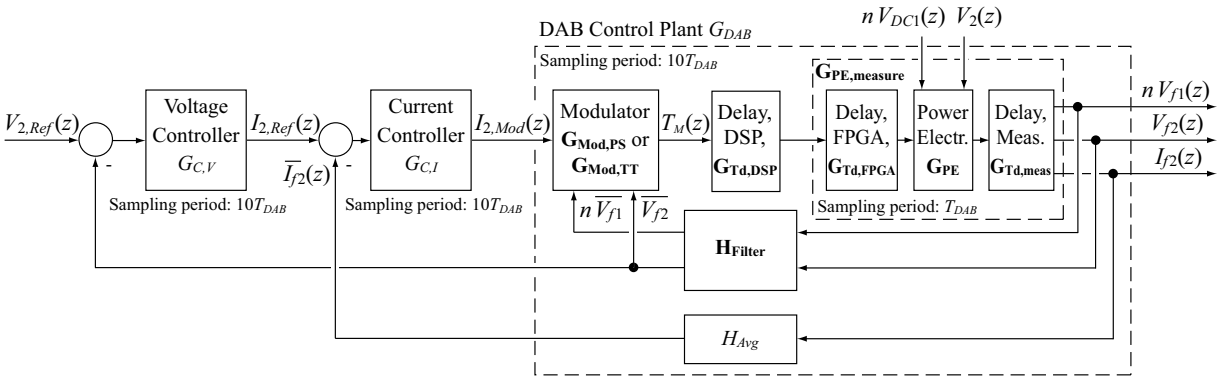

Figure 4: Investigated control structure with voltage and current control loops for power transfer from LV to HV port; gate signal generation (FPGA) as well as power electronics and measurements are sampled with sampling time T_{DAB}, therefore these three transfer functions need to be resampled to $10T_{DAB}$. The modulator output $T_M(z)$ depends on the employed modulation scheme. For phase shift modulation $T_M(z) = T_\varphi$, for the alternative modulation $\vec{T}_M(z) = (T_1,\ T_2,\ T_3)^{\mathrm{T}}$.

III. Small-Signal Model

Most blocks of the proposed control structure (**Figure 4**) are implemented in a Digital Signal Processor (DSP). This includes digital voltage and current controllers, as well as the modulator function ($G_{Mod,PS}$ or $G_{Mod,TT}$) which is used to calculate the required timing values for the DAB (e.g. T_φ for phase shift modulation based on (5)) with respect to the desired controller set value $I_{2,Mod}$ and the selected modulation scheme. Variations of these timing values dynamically alter the transferred power of the DAB power stage. The resulting changes of the filter currents $i_{f1}(t)$, $i_{f2}(t)$ and the filter voltages $v_{f1}(t)$, $v_{f2}(t)$ are obtained from the DAB small-signal model (the voltages V_{DC1} and V_2 remain approximately constant during one switching period T_S, since very large filter capacitors C_{DC1} and C_{DC2} are considered).

The full control diagram (Figure 4) indicates two transfer functions, that need to be determined in order to further investigate the control loop: the control to output transfer function G_{PE} of the DAB and the transfer function of the modulator.

A. DAB Power Stage, Phase Shift Modulation

Phase shift modulation is the most simple as well as the most common modulation method for the DAB. Therefore, the small-signal transfer function is first derived for this basic modulation scheme.

The small-signal calculation method outlined in [2] regards a single half cycle (e.g. $0 < t \le T_S/2$ in Figure 2) and separately considers the time intervals between two switching events (time intervals I and II in Figure 2). Within these time intervals, the time domain expressions for all system state variables (i.e. all time varying inductor currents and capacitor voltages) are required in order to determine its sensitivity on input signal variations. For the employed method, the state variables at the end of a half cycle are compared to the state variables at the beginning of the corresponding half cycle. This allows for the formulation of the control to output transfer function in discrete time domain.

Prior to the derivation of the transfer function, system inputs and outputs must be defined. Clearly, the timing parameter T_φ is an input to the dynamic system. Additionally, the voltages V_{DC1} and V_2 may be considered as inputs as well. The proposed system outputs are the filter current $i_{f2}(t) = i_{f2a}(t) + i_{f2b}(t)$ and the filter voltages $n \cdot v_{f1}(t)$, $v_{f2}(t)$. Further, it is reasonable to collect the system state variables in a state vector

$$\vec{x} = (i_L \quad i_{f1}/n \quad i_{f2a} \quad i_{f2b} \quad n\,v_{f1} \quad v_{f2})^{\mathrm{T}}\,. \tag{6}$$

In a next step, the time domain expressions for the system state variables need to be derived. These expressions remain the same during the time intervals indicated in Figure 2, however they may change at each switching time instant. For the sake of clarity the time domain expressions during each time interval i are combined to one single function

$$\begin{aligned}\vec{\mathrm{f}}_{\mathrm{PS},i}(\vec{x}_{i-1}, \Delta t) = \big(&i_{L,i}(\vec{x}_{i-1}, \Delta t) \quad i_{f1,i}(\vec{x}_{i-1}, \Delta t)/n \\ &i_{f2a,i}(\vec{x}_{i-1}, \Delta t) \quad i_{f2b,i}(\vec{x}_{i-1}, \Delta t) \\ &n\,v_{f1,i}(\vec{x}_{i-1}, \Delta t) \quad v_{f2,i}(\vec{x}_{i-1}, \Delta t)\big)^{\mathrm{T}}.\end{aligned} \tag{7}$$

In (7), Δt denotes the time within the considered time interval and $\vec{x}_{i-1}$ contains the initial values, so $\vec{\mathrm{f}}_{\mathrm{PS},i}(\vec{x}_{i-1}, 0) = \vec{x}_{i-1}$; the index "PS" denotes the phase shift modulation, the index i specifies the considered time interval. The analysis considers two different time intervals for phase shift modulation (Figure 2),

$$i = 1: \quad 0 < \Delta t \le T_\varphi\,, \tag{8}$$

$$i = 2: \quad T_\varphi < \Delta t + T_\varphi \le T_S/2\,. \tag{9}$$

The derivation of the time domain expressions in $\vec{\mathrm{f}}_{\mathrm{PS},i}(\vec{x}_{i-1}, \Delta t)$ is associated with a considerable calculation effort and is preferably carried out with a mathematical software tool which allows for symbolic evaluation (e.g. Mathematica, Maple).

In steady state, the system state vector $\vec{x}_{St}(t)$ (index "St" stands for "steady state") repeats cyclically every switching period. The steady state values of $\vec{x}_{St}(t)$ are obtained from

$$\vec{x}_{St}\left(t + \frac{T_S}{2}\right) = \begin{bmatrix} -1 & 0 & 0 & 0 & 0 & 0 \\ 0 & 1 & 0 & 0 & 0 & 0 \\ 0 & 0 & 1 & 0 & 0 & 0 \\ 0 & 0 & 0 & 1 & 0 & 0 \\ 0 & 0 & 0 & 0 & 1 & 0 \\ 0 & 0 & 0 & 0 & 0 & 1 \end{bmatrix} \cdot \vec{x}_{St}(t)\,, \tag{10}$$

since the DAB inductor current $i_L(t)$ changes its sign every half cycle in steady state [2] whereas the signs of the filter inductor currents and capacitor voltages remain the same after one half cycle. In order to solve for $\vec{x}_{St}(t)$ in (10), the time domain expressions for $\vec{x}(t + T_S/2)$ are required as a function of $\vec{x}(t)$. The derivation of these expressions

is described based on the switching sequence shown in Figure 2 and starts with the unknown values in $\vec{x}(t=0)$. With (7) and $i=1$, the general expression for $\vec{x}(t)$ at $t=T_\varphi$ is equal to

$$\vec{x}(T_\varphi) = \vec{\mathrm{f}}_{\mathrm{PS},1}\big(\vec{x}_0, T_\varphi\big) \text{ with } \vec{x}_0 = \vec{x}(0). \tag{11}$$

At $t=T_\varphi$ the switches T_5, T_6, T_7, and T_8 change and time interval II starts. Since capacitor voltages as well as inductor currents can not change instantaneously, the initial conditions of time interval II are equal to the final state variable values of time interval I, $\vec{x}_1 = \vec{x}(T_\varphi)$. With the time domain expressions for all state variables during time interval II the state vector at the end of the half cycle becomes

$$\begin{aligned}\vec{x}(T_S/2) = \vec{\mathrm{f}}_{\mathrm{PS},2}\big(\vec{x}_1, T_S/2 - T_\varphi\big) = \\ \vec{\mathrm{f}}_{\mathrm{PS},2}\Big(\vec{\mathrm{f}}_{\mathrm{PS},1}\big(\vec{x}(0), T_\varphi\big), T_S/2 - T_\varphi\Big).\end{aligned} \tag{12}$$

The steady state values are then obtained from the equation system (10) with (12), $\vec{x}_{St}(t) = \vec{x}(t)$, and $t=0$.

Besides for the calculation of the steady state, (12) as well forms the basis for the derivation of the discrete time small-signal model with sampling time

$$T_{DAB} = T_S/2 = 5\,\mu\mathrm{s}\,. \tag{13}$$

The proposed model considers small-signal deviations of the system state variables $\vec{x}(t)$ about the steady state $\vec{x}_{St}(t)$,

$$\hat{\vec{x}}(t) = \vec{x}(t) - \vec{x}_{St}(t) \tag{14}$$

(the symbol "$\hat{}$" denotes small-signal variables), by reason of three different kinds of excitations:

- variations of the state variables due to prior excitations of input variables: $\hat{\vec{x}}_0 = \hat{\vec{x}}(0) = \vec{x}(0) - \vec{x}_{St}(0)$
- LV and HV voltage changes: $\hat{\vec{v}}_{g,0} = (n\hat{V}_{DC1}(0)\ \ \hat{V}_2(0))^{\mathrm{T}}$
- excitation of the control input: $\hat{c}_{PS,0} = \hat{T}_\varphi(0)$

It is important to note, that the proposed discrete time model considers an excitation of any of these variables exactly at the beginning of the half cycle and calculates the respective values of the system state variables at the end of the half cycle. Consequently, all changes of the input variables $\hat{\vec{v}}_{g,0}(t)$ and $\hat{c}_{PS,0}(t)$ that occur for $t > 0$ are not at all considered in $\hat{\vec{x}}(T_{DAB})$. This limitation only regards transfer functions with continuous time input signals such as $V_{DC1}(t)$, $V_2(t)$. It does not affect the control to output transfer function in a digitally controlled system, provided that the digital controller is synchronized to the power electronics, so $T_\varphi(t)$ changes exactly at $t = k \cdot T_{DAB}$, $k \in \mathbb{N}_0$.

The small-signal deviations $\hat{\vec{x}}(T_{DAB})$ at the end of the half cycle are then obtained from a linear approximation [2],

$$\hat{\vec{x}}(T_{DAB}) \approx \mathbf{A}\cdot\hat{\vec{x}}_0 + \mathbf{B_{PS}}\cdot\hat{c}_{PS,0} + \mathbf{C}\cdot\hat{\vec{v}}_{g,0}, \tag{15}$$

whereas the three terms $\mathbf{A}\cdot\hat{\vec{x}}_0$, $\mathbf{B_{PS}}\cdot\hat{c}_{PS,0}$, and $\mathbf{C}\cdot\hat{\vec{v}}_{g,0}$ express the small-signal deviations of the state variables at $t = T_{DAB}$ as a result of excitations in $\hat{\vec{x}}_0$, $\hat{c}_{PS,0}$, and $\hat{\vec{v}}_{g,0}$, respectively. The expressions for $\mathbf{A}$, $\mathbf{B_{PS}}$, and $\mathbf{C}$ are given in Appendix A-A.

Expression (15) allows for the derivation of the required small-signal transfer functions: according to [2] and Appendix A-B, the z-domain control to output transfer functions are calculated with

$$\underset{3\times1}{\mathbf{G}}_{\mathbf{PE,PS}} = \begin{bmatrix} G_{PE,PS,I_{f2}} \\ G_{PE,PS,V_{f1}} \\ G_{PE,PS,V_{f2}} \end{bmatrix} = \mathbf{E}^{\mathrm{T}}\cdot(z_{DAB}\mathbf{I} - \mathbf{QRAQ})^{-1}\cdot\mathbf{QRB_{PS}}, \tag{16}$$

$$\underset{6\times6}{\mathbf{Q}} = \begin{bmatrix} \mathrm{sgn}(i_{L,0}) & \underset{1\times5}{\mathbf{0}} \\ \underset{5\times1}{\mathbf{0}} & \underset{5\times5}{\mathbf{I}} \end{bmatrix},\ \underset{6\times6}{\mathbf{R}} = \begin{bmatrix} -1 & \underset{1\times5}{\mathbf{0}} \\ \underset{5\times1}{\mathbf{0}} & \underset{5\times5}{\mathbf{I}} \end{bmatrix}, \tag{17}$$

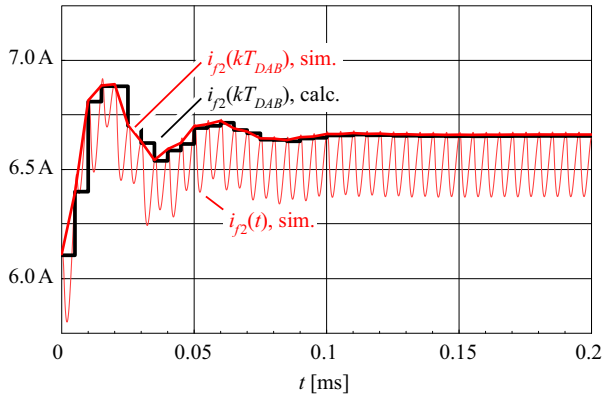

Figure 5: Simulated and calculated step response of $i_{f2}(t)$ for phase shift modulation, a time step of 100 ns, nominal operating point, and power being transferred from the LV to the HV port. The circuit simulator generates a continuous time waveform $i_{f2}(t)$ which is sampled after every half cycle, $t = k \cdot T_{DAB}$, in order to facilitate the comparison to the step response obtained from the discrete time small-signal transfer function $G_{PE,PS,I_{f2}}$.

and $z_{DAB} = \mathrm{e}^{sT_{DAB}}$.

In order for $\mathbf{G_{PE,PS}}$ to contain all control to output transfer functions for the output variables $I_{f2}(z_{DAB})$, $n\,V_{f1}(z_{DAB})$, and $V_{f2}(z_{DAB})$,

$$\underset{3\times1}{\mathbf{G}}_{\mathbf{PE,PS}} = \left[\frac{I_{f2a}(z_{DAB}) + I_{f2b}(z_{DAB})}{T_\varphi(z_{DAB})} \quad \frac{n\,V_{f1}(z_{DAB})}{T_\varphi(z_{DAB})} \quad \frac{V_{f2}(z_{DAB})}{T_\varphi(z_{DAB})}\right]^{\mathrm{T}}, \tag{18}$$

the matrix $\mathbf{E}^{\mathrm{T}}$ in (16) becomes

$$\mathbf{E}^{\mathrm{T}} = \begin{bmatrix} 0 & 0 & 1 & 1 & 0 & 0 \\ 0 & 0 & 0 & 0 & 1 & 0 \\ 0 & 0 & 0 & 0 & 0 & 1 \end{bmatrix}. \tag{19}$$

The small-signal transfer functions in (16) have been verified for various operating points with results from a circuit simulator (e.g. the control to output transfer function $G_{PE,PS,I_{f2}}$ in **Figure 5**). Simulated and calculated results show very good agreement for all investigated operating points.

B. DAB Power Stage, Alternative Modulation

When the DAB converter is operated within wide voltage ranges, its efficiency drops significantly for certain operating points when phase shift modulation used (i.e. for $V_2/V_1 \ll n$ or $V_2/V_1 \gg n$). The average DAB converter efficiency is considerably increased with an alternative modulation scheme [6], which is based on the modulation scheme with Triangular and Trapezoidal transformer current [7] (index "TT" denotes all variables regarding the alternative modulation).

The derivations of the small-signal transfer functions for phase shift modulation and alternative modulation are very similar. However, phase shift modulation requires only one control input T_φ whereas three control inputs T_1, T_2, and T_3 are needed for the alternative modulation.

Figure 3 depicts typical voltage and current waveforms for the DAB with alternative modulation. Again, one single half cycle is segmented into the time intervals where no switching occurs:

Interval I ($i=1$): $\quad 0 < \Delta t < T_1$,
Interval II ($i=2$): $\quad 0 < \Delta t < T_2$,
Interval III ($i=3$): $\quad 0 < \Delta t < T_3$,

Interval IV ($i = 4$): $0 < \Delta t < T_S/2 - (T_1 + T_2 + T_3)$.

This together with (6) and the time domain expressions for all state variables within time inverval i, $\vec{\mathrm{f}}_{\mathrm{TT},i}(\vec{x}_{i-1},\, \Delta t)$, (cf. (7)) facilitates the derivation of the system state values at the end of the half cycle,

$$\vec{x}(T_S/2) = \vec{\mathrm{f}}_{\mathrm{TT},4}\big(\vec{\mathrm{f}}_{\mathrm{TT},3}\big(\vec{\mathrm{f}}_{\mathrm{TT},2}\big(\vec{\mathrm{f}}_{\mathrm{TT},1}\big(\vec{x}(0),\, T_1\big),\, T_2\big),\, T_3\big),\, T_4\big) \tag{20}$$

whereas $T_4 = T_S/2 - (T_1 + T_2 + T_3)$.

The solution to the equation system formed with (10) and (20) determines the steady state values for $\vec{x}_{St}(t) = \vec{x}(t)$ at $t = 0$.

Equation (20) as well denotes the starting point for the small-signal transfer function derivation. In contrast to the phase shift modulation, the control input variable is now vector valued,

$$\hat{\vec{c}}_{TT,0} = (\hat{T}_1(0) \quad \hat{T}_2(0) \quad \hat{T}_3(0))^{\mathrm{T}}; \tag{21}$$

the small-signal vectors $\hat{\vec{x}}_0$ and $\hat{\vec{v}}_{g,0}$ remain unchanged. Consequently, the system states at the end of the half cycle can be approximately calculated with

$$\hat{\vec{x}}(T_{DAB}) \approx \mathbf{A} \cdot \hat{\vec{x}}_0 + \mathbf{B_{TT}} \cdot \hat{\vec{c}}_{TT,0} + \mathbf{C} \cdot \hat{\vec{v}}_{g,0}. \tag{22}$$

($\mathbf{A}$, $\mathbf{B_{TT}}$, and $\mathbf{C}$ are derived in Appendix A-A). The control to output transfer functions are collected in the matrix

$$\underset{3\times 3}{\mathbf{G}}_{\mathbf{PE,TT}} = \left[\vec{G}_{PE,TT,1} \quad \vec{G}_{PE,TT,2} \quad \vec{G}_{PE,TT,3}\right], \tag{23}$$

$$\vec{G}_{PE,TT,i} = \left(\frac{I_{f2a}(z_{DAB}) + I_{f2b}(z_{DAB})}{T_i(z_{DAB})} \quad \frac{n\,V_{f1}(z_{DAB})}{T_i(z_{DAB})} \quad \frac{V_{f2}(z_{DAB})}{T_i(z_{DAB})}\right)^{\mathrm{T}},$$

($i = 1, 2, 3$) which is derived based on (22) with (17) and (19),

$$\underset{3\times 3}{\mathbf{G}}_{\mathbf{PE,TT}} = \mathbf{E}^{\mathrm{T}} \cdot (z_{DAB}\mathbf{I} - \mathbf{QRAQ})^{-1} \cdot \mathbf{QRB_{TT}}. \tag{24}$$

The small-signal transfer functions in (23) have been verified with a circuit simulator. Very good agreement between simulation and calculation has been obtained for all investigated operating points (e.g. for nominal operation in **Figure 6** which shows the step response of the control to output transfer function $G_{PE,TT,1,I_{f2}}$ with input $T_1(z_{DAB})$ and output $I_{f2}(z_{DAB})$).

C. Modulator

The modulator calculates the control variables depending on the applied modulation scheme, the set current $I_{2,Mod}$, as well as the measured values $n\,\bar{V}_{f1}$ and $\bar{V}_{f2}$, obtained from $n\,V_{f1}$ and V_{f2}. The modulator function for phase shift modulation,

$$c_{PS} = T_\varphi = \mathrm{f}_{\mathrm{Mod,PS}}(i_{2,Mod}(t),\, n\,\bar{v}_{f1}(t),\, \bar{v}_{f2}(t)), \tag{25}$$

is derived in time domain from (5) for a lossless DAB. The expressions for the alternative modulation,

$$\vec{c}_{TT} = (T_1 \quad T_2 \quad T_3)^{\mathrm{T}} = \vec{\mathrm{f}}_{\mathrm{Mod,TT}}(i_{2,Mod}(t),\, n\,\bar{v}_{f1}(t),\, \bar{v}_{f2}(t)) \tag{26}$$

become rather large though, hence their evaluation in the DSP is avoided. Instead, precalculated values stored in DSP memory tables are used together with the fast linear interpolation algorithm presented in Appendix B. Since the modulator function is static, the small-signal transfer function is simply determined with the respective derivatives at the operating point. For phase shift modulation the transfer functions become

$$\underset{1\times 3}{\mathbf{G}}_{\mathbf{Mod,PS}} = \left[\frac{\partial \mathrm{f}_{\mathrm{Mod,PS}}}{\partial i_{2,Mod}} \quad \frac{\partial \mathrm{f}_{\mathrm{Mod,PS}}}{\partial (n\,\bar{v}_{f1})} \quad \frac{\partial \mathrm{f}_{\mathrm{Mod,PS}}}{\partial \bar{v}_{f2}}\right] \tag{27}$$

and for the alternative modulation

$$\underset{3\times 3}{\mathbf{G}}_{\mathbf{Mod,TT}} = \left[\frac{\partial \vec{\mathrm{f}}_{\mathrm{Mod,TT}}}{\partial i_{2,Mod}} \quad \frac{\partial \vec{\mathrm{f}}_{\mathrm{Mod,TT}}}{\partial (n\,\bar{v}_{f1})} \quad \frac{\partial \vec{\mathrm{f}}_{\mathrm{Mod,TT}}}{\partial \bar{v}_{f2}}\right]. \tag{28}$$

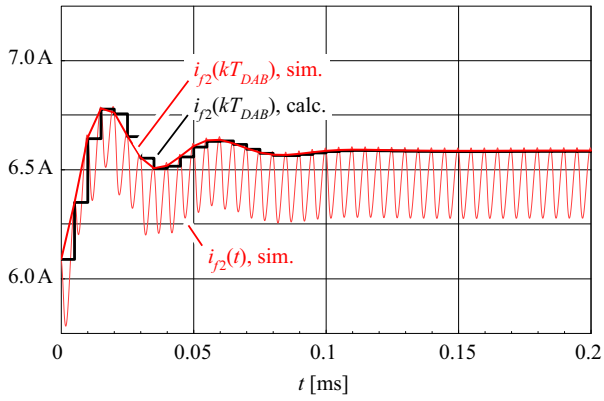

Figure 6: Simulated and calculated step response of $i_{f2}(t)$ when the alternative modulation is applied with a time step $\hat{T}_1 = 100\,\mathrm{ns} \cdot \sigma(t)$ and $\hat{T}_2 = \hat{T}_3 = 0$, nominal operation, and power being transferred from the LV to the HV port. The continuous time waveform $i_{f2}(t)$ is again sampled after every half cycle in order to facilitate the comparison to the step response obtained from the discrete time small-signal model.

$\mathbf{G_{Mod,PS}}$ and $\mathbf{G_{Mod,TT}}$ are evaluated at the operating point with given $i_{2,Mod}$ and the steady state values of $\bar{v}_{f1}$ and $\bar{v}_{f2}$ which are obtained from $\vec{x}_{St}(0)$.

IV. DAB Digital Control Loop

In the given laboratory setup, the DAB output voltage is controlled (e.g. V_{f2} in Figure 4 for power transfer from LV to HV). The proposed control loop consists of an inner loop with a PI-controller $G_{C,I}$ that controls $\bar{I}_{f2}(z)$ and an outer loop with another PI-controller $G_{C,V}$ which controls the output voltage. Depending on the power transfer direction, the output voltage can be either $V_{f2}(z)$ for power transfer from the LV port to the HV port or $n\,V_{f1}(z)$ for the opposite direction (the voltage control loop may be replaced by a voltage inspection algorithm in the final application where batteries are connected to LV and HV ports).

According to Figure 4, the current controller $G_{C,I}$ outputs $I_{2,Mod}(z)$ and connects to the modulator $\mathbf{G_{Mod}}$ (either $\mathbf{G_{Mod,PS}}$ or $\mathbf{G_{Mod,TT}}$, depending on the employed modulation algorithm). The modulator then calculates the DAB timing parameters in order to achieve the required power transfer. Since the current controller solely operates on the difference between $\bar{I}_{f2}(z)$ and $I_{2,ref}(z)$, G_{DAB} is a single input, single output transfer function with set current input $I_{2,Mod}(z)$ and HV side current output $\bar{I}_{f2}(z)$. However, there is internal feedback in the transfer function G_{DAB}, since $n\,\bar{V}_{f1}(z)$ and $\bar{V}_{f2}(z)$ are required for the modulator; this must be considered in order to determine G_{DAB}.

Except for the DAB small-signal transfer function matrix $\mathbf{G_{PE}}$ (equal to $\mathbf{G_{PE,PS}}$ or $\mathbf{G_{PE,TT}}$), all transfer functions in Figure 4 are part of the digital system and either reside in the DSP or in the FPGA. Relatively simple z-domain transfer functions result for the modulator $\mathbf{G_{Mod}}$ (Section III-C), the time delays $\mathbf{G_{Td,DSP}}$, $\mathbf{G_{Td,FPGA}}$, and $\mathbf{G_{Td,measure}}$, the moving average filters $\mathbf{H_{Filter}}$ and H_{Avg} as well as for the controllers $G_{C,V}$ and $G_{C,I}$. This section focuses on the transfer function details in order to allow for the derivation of G_{DAB}. The obtained transfer function is finally compared to a transfer function based on a simplified DAB model that allows for a significantly reduced calculation effort.

A. System Sampling Rate

The small-signal model of the power stage results in a z-domain transfer function with sampling time T_{DAB}. Due to the required DSP calculation time, the DAB timing parameters are only updated every $10\,T_{DAB}$, therefore the DSP sampling time is

$$T = 10\,T_{DAB} = 50\,\mu\text{s}, \quad z = \mathrm{e}^{sT}. \tag{29}$$

Hence, all transfer functions with faster update rate, such as $\mathbf{G_{PE}}$ and voltage and current measurements (Figure 4), need to be resampled according to Appendix C.

B. Time Delays

The implemented software acquires three measurements during one calculation period T in order to achieve higher noise immunity. The resulting time delay in $\mathbf{G_{Td,meas}}$ is $10\,T_{DAB}$ for the first measurement, $8\,T_{DAB}$ for the second and $6\,T_{DAB}$ for the third measurement. Additional time delay is caused from the FPGA ($\mathbf{G_{Td,FPGA}}$), which requires another $2\,T_{DAB}$ in order to apply the new timing values to the power electronics. FPGA and measurement time delays sum up to a total time delay of $12\,T$ for the first measurement, and $10\,T$ and $8\,T$ for the two subsequent measurements. The DSP calculates the average of the three measured values and

$$\mathbf{G_{PE,measure}}(z_{DAB}) = \frac{z_{DAB}^{-12} + z_{DAB}^{-10} + z_{DAB}^{-8}}{3} \cdot \mathbf{G_{PE}}(z_{DAB}) \tag{30}$$

results for that part of G_{DAB} which is updated with the higher sampling rate T_{DAB} (Figure 4). This transfer function finally needs to be resampled to the system sampling rate T according to Appendix C,

$$\mathbf{G_{PE,measure}}(z_{DAB}) \underset{\text{resample}}{\rightarrow} \mathbf{G_{r,PE,measure}}(z). \tag{31}$$

The DSP causes another time delay of T in order to carry out all calculations, therefore

$$G_{Td,DSP,PS}(z) = z^{-1}, \tag{32}$$

$$\mathbf{G_{Td,DSP,TT}}(z) = \mathrm{diag}\left(z^{-1}, z^{-1}, z^{-1}\right), \tag{33}$$

for phase shift or alternative modulation, respectively.

C. Moving Average Filters

The z-domain transfer function of the implemented N-th order moving average filter,

$$H_{Avg}(z) = \frac{1}{N} \sum_{i=0}^{N-1} z^{-i}, \tag{34}$$

calculates the average over N previously measured values $x(0),\ x(T) \ldots x((N-1)\cdot T)$; the present software implementation uses $N = 5$. The moving average filter is applied to $I_{f2}(z)$, $n\,V_{f1}(z)$, and $V_{f2}(z)$. The filter regarding I_{f2} is included in G_{DAB} (Section IV-D), and the feedback transfer function $\mathbf{H_{Filter}}$ contains the remaining two filter functions,

$$\mathbf{H_{Filter}}(z) = \mathrm{diag}\left(H_{Avg}, H_{Avg}\right). \tag{35}$$

D. DAB Control Plant G_{DAB}, Simplification

The transfer function G_{DAB} is calculated according to Appendix D,

$$G_{DAB} = \overline{I}_{f2}/I_{2,Mod} = H_{Avg}\left(G_{00} + \mathbf{G_{0r}H}\left(\mathbf{I} - \mathbf{G_{sr}H}\right)^{-1}\mathbf{G_{s0}}\right), \tag{36}$$

with G_{00}, $\mathbf{G_{0r}}$, $\mathbf{G_{sr}}$, and $\mathbf{G_{s0}}$ given in (56). According to Figure 4 and Figure 12, $\mathbf{G}$ and $\mathbf{H}$ become

$$\begin{aligned} \mathbf{G} &= \mathbf{G_{r,PE,measure,PS}} \cdot G_{Td,DSP,PS} \cdot \mathbf{G_{Mod,PS}}, \\ \mathbf{H} &= \mathbf{H_{Filter}} \end{aligned} \tag{37}$$

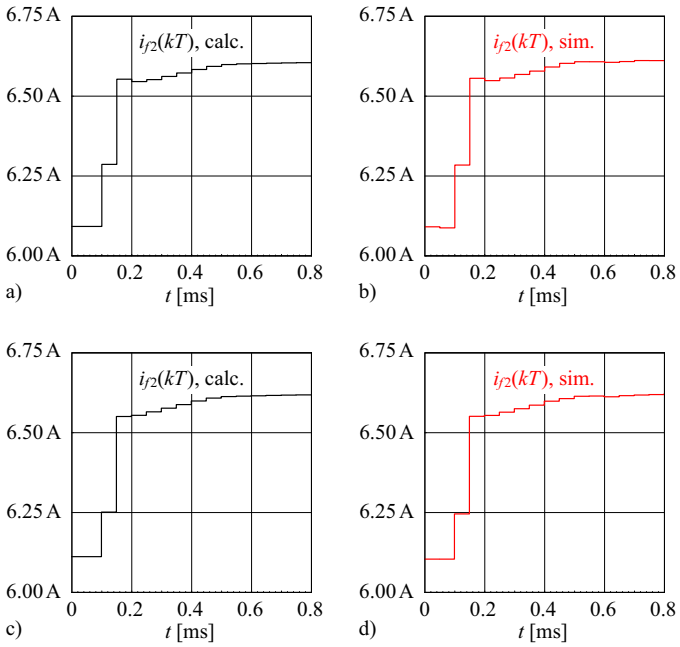

Figure 7: a) Calculated and b) simulated step response of $I_{f2}/I_{2,Mod} = G_{DAB}/H_{Avg}$ for phase shift operation; c) calculated and d) simulated step response of $I_{f2}/I_{2,Mod}$ when the alternative modulation is applied. The DAB is operated at nominal conditions with 2 kW being transferred from the LV to the HV port.

for phase shift modulation and

$$\begin{aligned} \mathbf{G} &= \mathbf{G_{r,PE,measure,TT}} \cdot \mathbf{G_{Td,DSP,TT}} \cdot \mathbf{G_{Mod,TT}}, \\ \mathbf{H} &= \mathbf{H_{Filter}} \end{aligned} \tag{38}$$

when the alternative modulation is employed.

G_{DAB} has been verified at various operating points using a circuit simulator; simulated and calculated step responses match very well for all investigated operating points, which is illustrated for nominal operation in **Figure 7**.

In the presented system, all time constants of the EMI filters are significantly smaller than the time delay caused by the digital controller. The question may arise, whether a simple DAB converter model would be sufficiently accurate in order to design current and voltage controllers. For steady state operation, the employed modulator functions $\mathbf{G_{Mod,PS}}$ or $\mathbf{G_{Mod,TT}}$ already generate almost correct timing parameters, i.e. $\overline{I}_{f2} \approx I_{2,Mod} \cdot G_{Td}$ (deviations occur due to the interpolation error and parasitic hardware components; G_{Td} considers the time delays caused from DSP, FPGA, and measurement), so the DAB converter in Figure 1 may be replaced with the two current sources in **Figure 8**. However, the simplified model may fail when $I_{2,Mod}$ changes, since the current $\overline{I}_{f2}$ depends on the actual values of $n\,\overline{V}_{f1}$ and $\overline{V}_{f2}$ as well. In **Figure 9**, the frequency response of G_{DAB} (phase shift modulation, nominal operation) is compared to the frequency response of the simplified transfer function $G_{DAB,simp}$ derived from the circuit depicted in Figure 8. Obviously, the frequency response obtained from the simplified model differs only little from the accurate model which is mainly due to the digital controller's time delays. Thorough investigations have shown that the simplified model and the accurate model match very well for phase shift modulation and alternative modulation as well as for all inspected operating points.

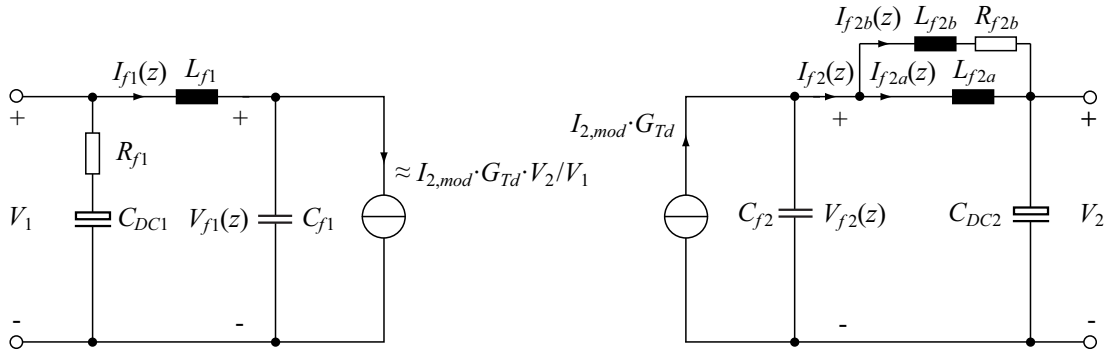

Figure 8: Simplified circuit of the DAB: current sources replace switches, inductor L, and transformer; for a lossless DAB, the accurate current for the source on the left side would be equal to $\mathcal{Z}\{i_{2,Mod}(t) \cdot v_{f2}(t)/v_{f1}(t)\} \cdot G_{Td}$ which is approximately equal to $I_{2,Mod}(z) \cdot G_{Td} \cdot V_2/V_1$ for constant voltages V_1, V_2 and when filter losses as well as variations of V_{f1} and V_{f2} are neglected. Since the simplified circuit contains no switches, it can directly be analyzed by means of Laplace- or Z-transform.

E. Current and Voltage Controllers

A constant output voltage is assumed since the load is considered as a voltage source, connected in parallel to the DC blocking capacitor. Therefore, and due to the modulator function (25) or (26), the DAB transfer function G_{DAB} is independent of the current operating point; G_{DAB} at nominal operation is considered for the design of current and voltage controllers.

For the current controller in Figure 4, a standard PI controller is proposed[1],

$$G_{C,I} = K_{p,I} \frac{z - (1 - T/T_{i,I})}{z - 1} \tag{39}$$

with gain $K_{p,I}$ and cut-off frequency $\omega_{i,I} = 1/T_{i,I}$. Consequently the open loop transfer function

$$F_{o,I} = G_{C,I} \cdot G_{DAB} \tag{40}$$

results. Since the transfer function G_{DAB} is similar to that of a low-pass filter, the following design method is proposed in order to achieve a high bandwidth of the closed current loop transfer function:

1) Calculation of the controller cut-off frequency such that $|G_{DAB}|$ at $\omega_{i,I}$ is 3 dB lower than the DC gain, i.e. $|G_{DAB}(z_{i,I})| = |G_{DAB}(\mathrm{e}^{j\cdot 0})|/\sqrt{2}$ with $z_{i,I} = \mathrm{e}^{j\omega_{i,I}T}$.
2) The controller gain $K_{p,I}$ is determined in order to achieve a given phase margin Φ_R. First, the z-Parameter z_{Φ_R} needs to be determined where the open loop phase equals $-180^\circ + \Phi_R$, $\arg(F_{o,I}(z_{\Phi_R})/K_{p,I}) = -180^\circ + \Phi_R$. With this, the controller gain $K_{p,I} = |K_{p,I}/F_{o,I}(z_{\Phi_R})|$ can be calculated.

With $\Phi_R = 60^\circ$, the controller parameters $K_{p,I} = 0.42$ and $T_{i,I} = 129\,\mu\mathrm{s}$ result for the given system setup; in **Figure 10** the step response of the closed current control loop is depicted.

The direction of power transfer determines the voltage that needs to be controlled: this is V_1 for power transfer from the HV to the LV port, and V_2 for the opposite direction. In the given system V_1 and V_2 are not measured, therefore the approximations $V_1 \approx V_{f1}$ and $V_2 \approx V_{f2}$ are used in order to design the voltage controller (this approximation is sufficiently accurate for the voltage control loop, since the EMI filter time constants are much smaller than the control loop time constants). The voltage controller again consists of a PI controller with transfer function

$$G_{C,V} = K_{p,V} \frac{z - (1 - T/T_{i,V})}{z - 1}. \tag{41}$$

For power being transferred from the LV to the HV port, the controlled current I_{f2} flows into the output capacitor C_{DC2} and the load. The plant transfer function for the voltage controller then consists of the closed current loop transfer function, the capacitor C_{DC2}, and the load connected to the HV port. When the direction of power transfer changes (HV to LV), then the current I_{f1}, which is not measured in the given system, flows into C_{DC1} and into the

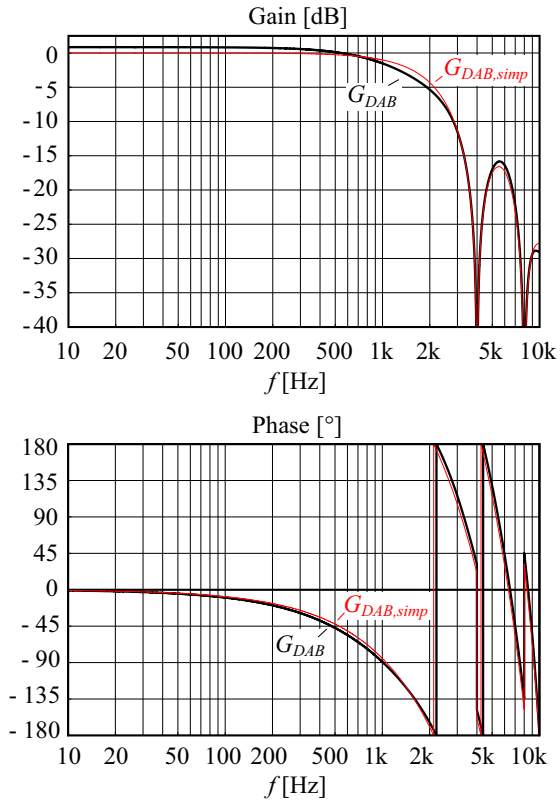

Figure 9: Frequency response of the accurate and the simplified transfer functions G_{DAB} and $G_{DAB,simp}$, respectively.

[1]The digital PI controller is obtained from its continuous time counterpart [8].

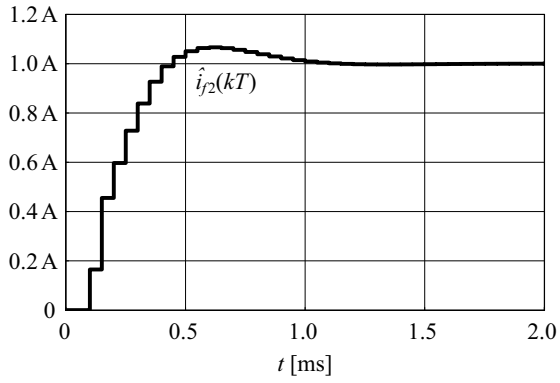

Figure 10: Unity step response of the closed current control loop; a rise time of less than $500\,\mu s$ is achieved.

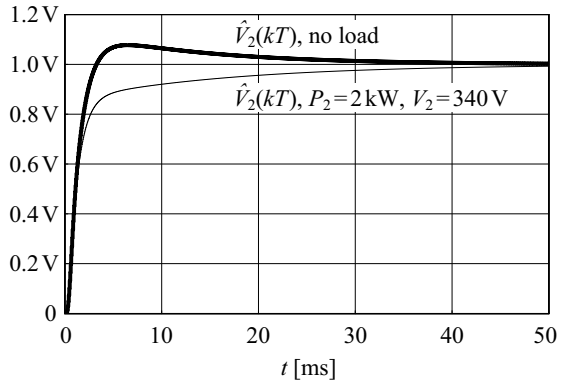

Figure 11: Unity step response of the closed voltage control loop for no-load operation and for $2\,\mathrm{kW}$ output power at $340\,\mathrm{V}$ output voltage.

load connected to the LV port. However, I_{f1} can be approximated with $I_{f2} \cdot V_2/V_1$ for control purposes, since losses are rather low and the capacitance of C_{DC1} is comparably large. The transfer function of the closed current loop again exhibits low-pass characteristics but the output capacitor, as well as the load in case of a voltage source type load, add an integration stage to the plant. For this type of plant, the "symmetric optimum" design method [9] is proposed in order to design the voltage controller (in the case of a resistive load, the no-load operation depicts the worst case for the voltage controller design). A phase margin of $\Phi_R = 75^\circ$ leads to $K_{p,V} = 71\,\mathrm{mA/V}$ and $T_{i,I} = 14.5\,\mathrm{ms}$ with the step responses of the system depicted in **Figures 11** for no load and for a load resistance of $58\,\Omega \approx (340\,\mathrm{V})^2/2\,\mathrm{kW}$.

V. Conclusion

To develop an accurate small-signal model for a DAB converter, a precise knowledge of the modulation method is required and the EMI filters need to be included in order to consider their interactions with the DAB. However, simplified converter models may be used in order to facilitate a less extensive controller design, since the time delay of a digitally controlled system causes a significant phase lag, which is considerably larger than the power converter's phase lag.

In this paper, two small-signal models for the DAB including EMI filter and different modulation schemes are derived. Further, the structure of the digital control system (including the most relevant algorithms), a simplified DAB model as well as the controller design are extensively described.

Even though the focus is on the DAB, the proposed small-signal model derivation method as well as the given digital control structure could easily be extended in order to enable precise control of arbitrary resonant power converters with unidirectional and bidirectional power flow.

Appendix A
Small-Signal Model

A. Matrix Expressions (from [2])

The state space matrix $\mathbf{A}$ for phase shift modulation (15) contains the derivatives of all system state variables at the end of the half cycle, $\vec{x}(t = T_{DAB})$, with respect to the state variables at the beginning of the half cycle, $\vec{x}(t = 0)$,

$$\mathbf{A} = \lim_{t \to T_{DAB}} \begin{bmatrix} \frac{\partial i_L}{\partial i_{L,0}} & \frac{\partial i_L}{\partial (i_{f1,0}/n)} & \frac{\partial i_L}{\partial i_{f2a,0}} & \frac{\partial i_L}{\partial i_{f2b,0}} & \frac{\partial i_L}{\partial (n v_{f1,0})} & \frac{\partial i_L}{\partial v_{f2,0}} \\ \frac{\partial (i_{f1}/n)}{\partial i_{L,0}} & \frac{\partial (i_{f1}/n)}{\partial (i_{f1,0}/n)} & \frac{\partial (i_{f1}/n)}{\partial i_{f2a,0}} & \frac{\partial (i_{f1}/n)}{\partial i_{f2b,0}} & \frac{\partial (i_{f1}/n)}{\partial (n v_{f1,0})} & \frac{\partial (i_{f1}/n)}{\partial v_{f2,0}} \\ \frac{\partial i_{f2a}}{\partial i_{L,0}} & \frac{\partial i_{f2a}}{\partial (i_{f1,0}/n)} & \frac{\partial i_{f2a}}{\partial i_{f2a,0}} & \frac{\partial i_{f2a}}{\partial i_{f2b,0}} & \frac{\partial i_{f2a}}{\partial (n v_{f1,0})} & \frac{\partial i_{f2a}}{\partial v_{f2,0}} \\ \frac{\partial i_{f2b}}{\partial i_{L,0}} & \frac{\partial i_{f2b}}{\partial (i_{f1,0}/n)} & \frac{\partial i_{f2b}}{\partial i_{f2a,0}} & \frac{\partial i_{f2b}}{\partial i_{f2b,0}} & \frac{\partial i_{f2b}}{\partial (n v_{f1,0})} & \frac{\partial i_{f2b}}{\partial v_{f2,0}} \\ \frac{\partial (n v_{f1})}{\partial i_{L,0}} & \frac{\partial (n v_{f1})}{\partial (i_{f1,0}/n)} & \frac{\partial (n v_{f1})}{\partial i_{f2a,0}} & \frac{\partial (n v_{f1})}{\partial i_{f2b,0}} & \frac{\partial (n v_{f1})}{\partial (n v_{f1,0})} & \frac{\partial (n v_{f1})}{\partial v_{f2,0}} \\ \frac{\partial v_{f2}}{\partial i_{L,0}} & \frac{\partial v_{f2}}{\partial (i_{f1,0}/n)} & \frac{\partial v_{f2}}{\partial i_{f2a,0}} & \frac{\partial v_{f2}}{\partial i_{f2b,0}} & \frac{\partial v_{f2}}{\partial (n v_{f1,0})} & \frac{\partial v_{f2}}{\partial v_{f2,0}} \end{bmatrix}, \tag{42}$$

and is evaluated at the steady state operating point $\vec{x}_{St}(0)$. $\mathbf{B_{PS}}$ and $\mathbf{C}$ contain the derivatives of $\vec{x}(t = T_{DAB})$ with respect to the input variables,

$$\mathbf{B_{PS}} = \lim_{t \to T_{DAB}} \begin{bmatrix} \frac{\partial i_L}{\partial T_{\varphi,0}} \\ \frac{\partial (i_{f1}/n)}{\partial T_{\varphi,0}} \\ \frac{\partial i_{f2a}}{\partial T_{\varphi,0}} \\ \frac{\partial i_{f2b}}{\partial T_{\varphi,0}} \\ \frac{\partial (n v_{f1})}{\partial T_{\varphi,0}} \\ \frac{\partial v_{f2}}{\partial T_{\varphi,0}} \end{bmatrix} \quad \text{and} \quad \mathbf{C} = \lim_{t \to T_{DAB}} \begin{bmatrix} \frac{\partial i_L}{\partial V_{1,0}} & \frac{\partial i_L}{\partial V_{2,0}} \\ \frac{\partial (i_{f1}/n)}{\partial V_{1,0}} & \frac{\partial (i_{f1}/n)}{\partial V_{2,0}} \\ \frac{\partial i_{f2a}}{\partial V_{1,0}} & \frac{\partial i_{f2a}}{\partial V_{2,0}} \\ \frac{\partial i_{f2b}}{\partial V_{1,0}} & \frac{\partial i_{f2b}}{\partial V_{2,0}} \\ \frac{\partial (n v_{f1})}{\partial V_{1,0}} & \frac{\partial (n v_{f1})}{\partial V_{2,0}} \\ \frac{\partial v_{f2}}{\partial V_{1,0}} & \frac{\partial v_{f2}}{\partial V_{2,0}} \end{bmatrix}. \tag{43}$$

For the alternative modulation (22), $\mathbf{A}$ and $\mathbf{C}$ are again derived according to (42) and (43), only $\mathbf{B_{PS}}$ changes to $\mathbf{B_{TT}}$,

$$\mathbf{B_{TT}} = \lim_{t \to T_{DAB}} \begin{bmatrix} \frac{\partial i_L}{\partial T_{1,0}} & \frac{\partial i_L}{\partial T_{2,0}} & \frac{\partial i_L}{\partial T_{3,0}} \\ \frac{\partial (i_{f1}/n)}{\partial T_{1,0}} & \frac{\partial (i_{f1}/n)}{\partial T_{2,0}} & \frac{\partial (i_{f1}/n)}{\partial T_{3,0}} \\ \frac{\partial i_{f2a}}{\partial T_{1,0}} & \frac{\partial i_{f2a}}{\partial T_{2,0}} & \frac{\partial i_{f2a}}{\partial T_{3,0}} \\ \frac{\partial i_{f2b}}{\partial T_{1,0}} & \frac{\partial i_{f2b}}{\partial T_{2,0}} & \frac{\partial i_{f2b}}{\partial T_{3,0}} \\ \frac{\partial (n v_{f1})}{\partial T_{1,0}} & \frac{\partial (n v_{f1})}{\partial T_{2,0}} & \frac{\partial (n v_{f1})}{\partial T_{3,0}} \\ \frac{\partial v_{f2}}{\partial T_{1,0}} & \frac{\partial v_{f2}}{\partial T_{2,0}} & \frac{\partial v_{f2}}{\partial T_{3,0}} \end{bmatrix}. \tag{44}$$

$\mathbf{B_{PS}}$, $\mathbf{B_{TT}}$, and $\mathbf{C}$ are again evaluated at the steady state operating point $\vec{x}_{St}(0)$.

B. Small-Signal Transfer Function

The z-domain control to output transfer function is derived with equations (71) and (74) in [2],

$$\mathbf{G} = \mathbf{E}^{\mathrm{T}} \cdot (z_{DAB}\mathbf{I} - \mathbf{Q}(k)\mathbf{R}\mathbf{P}(k)\mathbf{A}\mathbf{P}(k)\mathbf{Q}(k))^{-1} \cdot \mathbf{Q}(k)\mathbf{R}\mathbf{P}(k)\mathbf{B}_{\mathbf{PS}}, \tag{45}$$

with $\mathbf{R}$ defined in (17) in this paper, an integer number k and

$$\underset{6\times6}{\mathbf{P}}(k) = \begin{bmatrix} (-1)^k & \underset{1\times5}{\mathbf{0}} \\ \underset{5\times1}{\mathbf{0}} & \underset{5\times5}{\mathbf{I}} \end{bmatrix}, \ \underset{6\times6}{\mathbf{Q}}(k) = \begin{bmatrix} (-1)^k \cdot \mathrm{sgn}(i_{L,0}) & \underset{1\times5}{\mathbf{0}} \\ \underset{5\times1}{\mathbf{0}} & \underset{5\times5}{\mathbf{I}} \end{bmatrix}. \tag{46}$$

The products $\mathbf{P}(k)\mathbf{Q}(k)$ and $\mathbf{Q}(k)\mathbf{R}\mathbf{P}(k)$ are equal to

$$\begin{aligned} \mathbf{Q}(k)\mathbf{R}\mathbf{P}(k) &= \begin{bmatrix} -\mathrm{sgn}(i_{L,0}) & \underset{1\times5}{\mathbf{0}} \\ \underset{5\times1}{\mathbf{0}} & \underset{5\times5}{\mathbf{I}} \end{bmatrix} = \mathbf{Q}(0)\,\mathbf{R}, \\ \mathbf{P}(k)\mathbf{Q}(k) &= \begin{bmatrix} \mathrm{sgn}(i_{L,0}) & \underset{1\times5}{\mathbf{0}} \\ \underset{5\times1}{\mathbf{0}} & \underset{5\times5}{\mathbf{I}} \end{bmatrix} = \mathbf{Q}(0) \text{ for } k \in \mathbb{Z}, \end{aligned} \tag{47}$$

and thus independent on k which allows for the simplified representation (16), (17).

Appendix B
Fast Linear Interpolation Algorithm

The modulator functions discussed in Section III-C contain three parameters. Consequently, a 3-D table is required to store the basic values; an appropriate algorithm then interpolates the function values between the basic values.

In order to develop the 3-D interpolation algorithm, the proposed interpolation algorithm is first discussed based on the data of a 2-D table with x- and y-axis and is then extended to 3-D. For the sake of clarity, the input values to the underlying 2-D function $\mathrm{f}(x, y)$ are confined to $0 \le x \le 1$ and $0 \le y \le 1$ with four surrounding basic values $\mathrm{f}(0,0)$, $\mathrm{f}(0,1)$, $\mathrm{f}(1,0)$, and $\mathrm{f}(1,1)$, obtained from the 2-D table. The interpolated function values at $x = 0$ and $x = 1$ are calculated using linear expressions,

$$\begin{aligned} \mathrm{f_i}(0, y) &= \mathrm{f}(0,0) + [\mathrm{f}(0,1) - \mathrm{f}(0,0)] \cdot y, \\ \mathrm{f_i}(1, y) &= \mathrm{f}(1,0) + [\mathrm{f}(1,1) - \mathrm{f}(1,0)] \cdot y. \end{aligned}$$

The obtained values $\mathrm{f_i}(0, y)$ and $\mathrm{f_i}(1, y)$ are then used to calculate the interpolated function value $\mathrm{f_i}(x, y)$,

$$\mathrm{f_i}(x, y) = \mathrm{f_i}(0, y) + [\mathrm{f_i}(1, y) - \mathrm{f_i}(0, y)] \cdot x. \tag{48}$$

This method can easily be extended to a 3-D function $\mathrm{f}(x, y, z)$ with $0 \le x \le 1$, $0 \le y \le 1$, and $0 \le z \le 1$ as well as 8 surrounding table values $\mathrm{f}(0,0,0) \ \ldots \ \mathrm{f}(1,1,1)$,

$$\begin{aligned} \mathrm{f_i}(0,0,z) &= \mathrm{f}(0,0,0) + [\mathrm{f}(0,0,1) - \mathrm{f}(0,0,0)] \cdot z, \\ \mathrm{f_i}(0,1,z) &= \mathrm{f}(0,1,0) + [\mathrm{f}(0,1,1) - \mathrm{f}(0,1,0)] \cdot z, \\ \mathrm{f_i}(1,0,z) &= \mathrm{f}(1,0,0) + [\mathrm{f}(1,0,1) - \mathrm{f}(1,0,0)] \cdot z, \\ \mathrm{f_i}(1,1,z) &= \mathrm{f}(1,1,0) + [\mathrm{f}(1,1,1) - \mathrm{f}(1,1,0)] \cdot z, \\ \\ \mathrm{f_i}(0,y,z) &= \mathrm{f_i}(0,0,z) + [\mathrm{f_i}(0,1,z) - \mathrm{f_i}(0,0,z)] \cdot y, \\ \mathrm{f_i}(1,y,z) &= \mathrm{f_i}(1,0,z) + [\mathrm{f_i}(1,1,z) - \mathrm{f_i}(1,0,z)] \cdot y, \\ \\ \mathrm{f_i}(x,y,z) &= \mathrm{f_i}(0,y,z) + [\mathrm{f_i}(1,y,z) - \mathrm{f_i}(0,y,z)] \cdot x. \end{aligned} \tag{49}$$

The calculation of $\mathrm{f_i}(x, y, z)$ requires a total of 7 multiplications and 14 additions or subtractions.

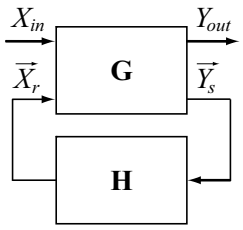

Figure 12: Single input, single output system with internal feedback used to derive G_{DAB}.

Appendix C
Sampling Rate Reduction

For a given discrete time system with sampling rate T, step response function $h(kT)$, $k \in \mathbb{N}_0$, and corresponding z-domain transfer function $G(z)$, the transfer function $G_r(z)$ with increased sampling time $T_r = N \cdot T$, $N \in \mathbb{N}$ and similar step response function $h_r(kT_r) = h(kNT)$, is derived.

The original z-domain transfer function

$$G(z) = \frac{a(z)}{b(z)} \tag{50}$$

contains two polynomials $a(z)$ and $b(z)$ with constant and real coefficients and $\deg(a(z)) < \deg(b(z))$.

Based on the relation between the i-th pole $p_{s,i}$ of a continuous time transfer function and the i-th pole $p_{z,i}$ of the corresponding discrete time transfer function [10],

$$p_{z,i} = \mathrm{e}^{p_{s,i}T}, \tag{51}$$

the i-th pole $p_{rz,i}$ of $G_r(z)$ can be expressed as

$$p_{rz,i} = \mathrm{e}^{p_{s,i}T_r} = \mathrm{e}^{p_{s,i}NT} = p_{z,i}^N. \tag{52}$$

The method discussed in [10] then represents a simple way to obtain the numerator $a_r(z)$ of $G_r(z)$ based on the step response $h_r(kT_r)$ of the corresponding time domain function which is equal to the step response of the already known function $h(k_N T)$ for $k_N = N \cdot k$ (this can be achieved with the Matlab command `d2d` as well).

Appendix D
Derivation of G_{DAB}

For the sake of clarity, the derivation of G_{DAB} is based on a simplified single input, single output system with input X_{in} and output Y_{out} in **Figure 12**. It contains the multiple input, multiple output transfer function $\mathbf{G}(z)$ in the forward path and $\mathbf{H}(z)$ in the feedback path. Vector $\vec{X}$ denotes the input of $\mathbf{G}(z)$,

$$\vec{X} = \begin{pmatrix} X_{in} & \vec{X}_r^{\mathrm{T}} \end{pmatrix}^{\mathrm{T}}, \quad \vec{X}_r \in \mathbb{R}^n \tag{53}$$

with the system input value X_{in} and internal system values in $\vec{X}_r$. The output of $\mathbf{G}(z)$,

$$\vec{Y} = \mathbf{G} \cdot \vec{X} = \begin{pmatrix} Y_{out} & \vec{Y}_s^{\mathrm{T}} \end{pmatrix}^{\mathrm{T}}, \quad \vec{Y}_s \in \mathbb{R}^m. \tag{54}$$

contains Y_{out} and another set of internal system values $\vec{Y}_s$ that denote the input values of $\mathbf{H}(z)$. The output of $\mathbf{H}(z)$ is then equal to $\vec{X}_r$,

$$\vec{X}_r = \underset{n\times m}{\mathbf{H}} \cdot \vec{Y}_s, \tag{55}$$

in order to close the feedback loop. The transfer function matrix $\mathbf{G}$ is split up into

$$\mathbf{G} = \begin{bmatrix} G_{00} & \underset{1\times n}{\mathbf{G_{0r}}} \\ \underset{m\times 1}{\mathbf{G_{s0}}} & \underset{m\times n}{\mathbf{G_{sr}}} \end{bmatrix}. \tag{56}$$

With (53), (54), (55) and (56) the system output value $\vec{Y}_{out}$ and the vector $\vec{Y}_s$ become

$$Y_{out} = G_{00}X_{in} + \mathbf{G_{0r}}\vec{X}_r = G_{00}X_{in} + \mathbf{G_{0r}H}\vec{Y}_s \tag{57}$$

$$\vec{Y}_s = \mathbf{G_{s0}}X_{in} + \mathbf{G_{sr}}\vec{X}_r = \mathbf{G_{s0}}X_{in} + \mathbf{G_{sr}H}\vec{Y}_s \tag{58}$$

and thus

$$\vec{Y}_s = \left(\mathbf{I} - \mathbf{G_{sr}H}\right)^{-1}\mathbf{G_{s0}}X_{in}. \tag{59}$$

Based on (57) and (59) the system transfer function G_{DAB} results in

$$G_{DAB} = Y_{out}/X_{in} = G_{00} + \mathbf{G_{0r}H}\left(\mathbf{I} - \mathbf{G_{sr}H}\right)^{-1}\mathbf{G_{s0}}. \tag{60}$$

REFERENCES

[1] R.W. Erickson, D. Maksimović, "Fundamentals of Power Electronics," 2nd edition, New York: Springer, 2001.

[2] I. Batarseh and K. Siri, "Generalized Approach to the Small Signal Modeling of DC-to-DC Resonant Converters," *IEEE Trans. Aerospace and Electronic Systems*, vol. 29, no. 3, pp. 894–909, 1993.

[3] A. Emadi, S.S. Williamson, and A. Khaligh, "Power Electronics Intensive Solutions for Advanced Electric, Hybrid Electric, and Fuel Cell Vehicular Power Systems," *IEEE Trans. Power Electron.*, vol. 21, no. 3, pp. 567–577, 2006.

[4] S. Inoue and H. Akagi, "A Bidirectional Isolated DC-DC Converter as a Core Circuit of the Next-Generation Medium-Voltage Power Conversion System," *IEEE Trans. Power Electron.*, vol. 22, no. 2, pp. 535–542, 2007.

[5] M.H. Kheraluwala, R.W. Gascoigne, D.M. Divan, and E.D. Baumann, "Performance Characterization of a High-Power Dual Active Bridge dc-to-dc Converter," *IEEE Trans. Ind. Appl.*, vol. 28, no. 6, pp. 1294–1301, 1992.

[6] F. Krismer, S. Round, J.W. Kolar, "Performance Optimization of a High Current Dual Active Bridge with a Wide Operating Voltage Range," in *Proc. 37th IEEE PESC*, Jeju, Korea, June 18–22, 2006, pp. 1–7.

[7] N. Schibli, "Symmetrical multilevel converters with two quadrant DC-DC feeding," PhD thesis no. 2220, EPFL Lausanne, 2000.

[8] G.F. Franklin, J.D. Powell, and M.L. Workman, "Digital Control of Dynamic Systems," 3rd edition, Menlo Park, CA: Addison Wesley Longman, 1998.

[9] J.W. Umland and M. Safiuddin, "Magnitude and Symmetric Optimum Criterion for the Design of Linear Control Systems: What Is It and How Does It Compare with the Others?," *IEEE Trans. Ind. Appl.*, vol. 26, no. 3, pp. 489–496, 1990.

[10] P.N. Robinson and G.S. Robinson, "A Computer Method for Obtaining z Transforms," *IEEE Trans. on Audio and Electroacoustics*, vol. 20, no. 1, pp. 98–99, 1972.